POAC'25
St. John's, Newfoundland and Labrador, Canada

Proceedings of the 28th International Conference on Port and Ocean Engineering under Arctic Conditions
Jul 13-17, 2025
St. John's, Newfoundland and Labrador
Canada

Design of a Novel Test Apparatus for Assessing the Effectiveness of Air Bubbler System in Reducing Ice Hull Resistance

Noah M. Osmond[1], Rocky S. Taylor[1], Jungyong Wang[2]
[1] Faculty of Engineering and Applied Science, Memorial University of Newfoundland, St. John's, NL Canada
[2] National Research Council, Ocean, Coastal, and River Engineering (NRC-OCRE), St. John's, Canada

ABSTRACT

Full-scale operations with vessels like the CCGS Henry Larsen have shown that air bubbler systems can enhance ship performance in sea ice. However, quantifying the effectiveness of these systems in reducing hull resistance remains a challenge, as conventional friction board tests are inadequate for evaluating air bubbler technologies. To address this gap, we have developed a novel model-scale friction board testing apparatus and methodology. This apparatus features a friction board mounted on six load cells that constrain all degrees of freedom, enabling accurate measurement of ice loading and frictional forces during ice-hull interactions. A specially designed box, equipped with a pressure plate on pneumatic pistons, applies controlled force through brash ice onto the friction board as the box translates along its length. A multi-port air bubbler system is integrated beneath the board to provide variable air flow as needed. This setup allows for systematic testing under controlled conditions, with adjustable parameters such as ice pressure, simulated ship speed, and air bubbler flow rate. This paper describes the apparatus design, the testing methodology, and preliminary findings obtained with the new equipment. In a companion paper, results from a systematic investigation of the effects of ice pressure, ship speed and air flow rate are presented.

KEY WORDS: Air bubbler; Friction board; Model-scale; Load cells; Brash ice

INTRODUCTION

The testing of ice hull friction is a complex area of study. The use of specialized equipment and methods for the purpose of evaluating ship hull resistance and associated interactions with ice have been researched in terms of full-scale and model-scale correlation (Spencer & Jones, 2001; Lau, 2015). However, testing procedures for other scenarios such as air bubbler effects have yet to be fully developed. To this end, the present work was carried out to develop a systematic way of evaluating the effectiveness and performance of air bubbler systems, and to provide new insights into the physics associated with this complex phenomenon. By designing a test apparatus that could be used to assess dependence of performance on key inputs, this work aims to support the development technology for improving the performance of ships operating in ice. This paper summarizes the design and functionality of a novel testing

apparatus, capable of evaluating scenarios involving air bubbler systems. The apparatus design allows for the control of key inputs: simulated ship speed (ice box speed), air bubbler flow rate, and pack ice pressure (applied mean ice pressure).

To achieve this, a sensitive dynamometer was incorporated into the design which is capable of isolating and measuring changes in ice friction forces on a friction board fitted with an air bubbler system. Prior work has shown that the evaluation of an air bubbler system using the standard friction board method was not suitable (Browne & Wang, 2023; Hill, 2008; Marmo et al., 2005). The design of this apparatus was intended to solve identified shortcomings of the traditional friction board implementation by allowing the air bubbles to move vertically and agitate the water, so as to provides a more accurate representation of the full-scale process (Juurmaa, 1978; Wang et al., 2023; Wilkman, 2011). The design incorporated a vertically mounted friction board and a moving box (ice box) containing brash ice. A set of pneumatic pistons in the ice box allows for the ice to be forced into the friction board at a specified level, simulating pack ice pressure. The apparatus used flex links, in conjunction with load cells to constrain the six degrees of freedom and record the force in each. Rather than just evaluating ice friction in a single axis, a fully constrained design such as this can provide a more complete model. This allows for a greater and more holistic understanding around the air bubbler system affects.

APPARATUS DESIGN

The apparatus was designed to be installed within a portable, transparent ice rubble test tank measuring 3 m × 0.91 m × 0.61 m. The tank, along with the complete test apparatus, is shown in Figure 1 and Figure 2. The main apparatus frame, depicted in Figure 3, was engineered to rest along the top edge of the tank, supporting the entire testing system, including the friction board assembly, ice box, and air bubbler system, as well as all forces generated during testing. The frame was secured within slots on the top of the tank to prevent movement and was further reinforced using C-clamps. Constructed from solid 40 mm 80/20 T-slot rails, the frame was additionally strengthened with three 2 × 2-inch rectangular steel tubing cross members mounted across the top. Structural rigidity was essential, as even minimal flexing could introduce inaccuracies in the recorded data.

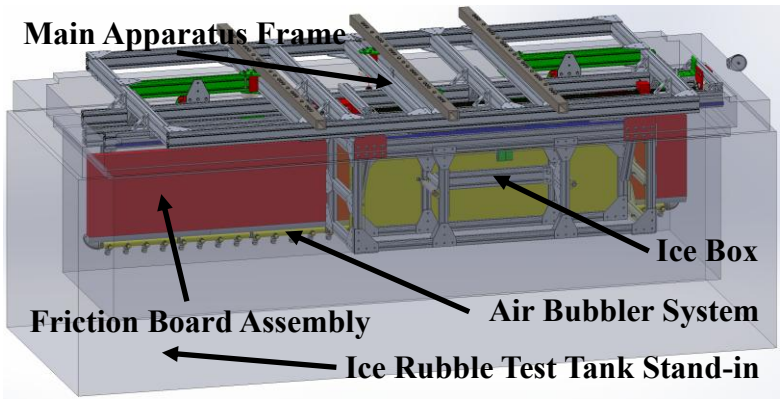

Figure 1. Tank stand-in and full testing apparatus

Figure 2. Tank and test frame

The ice box was suspended from the frame and traveled along a set of 15 mm ball-bearing carriage rails, as shown in Figure 3. This configuration allowed the ice box to move along the length of the tank parallel to the friction board. To ensure accurate load cell data acquisition,

the flex links and load cells were mounted on the friction board assembly. This design choice effectively isolated the load cells from vibrations and movement generated by the ice box and motor assemblies. Additionally, the design helped mitigate hydrodynamic forces acting on the system, allowing for more precise isolation of ice loading effects.

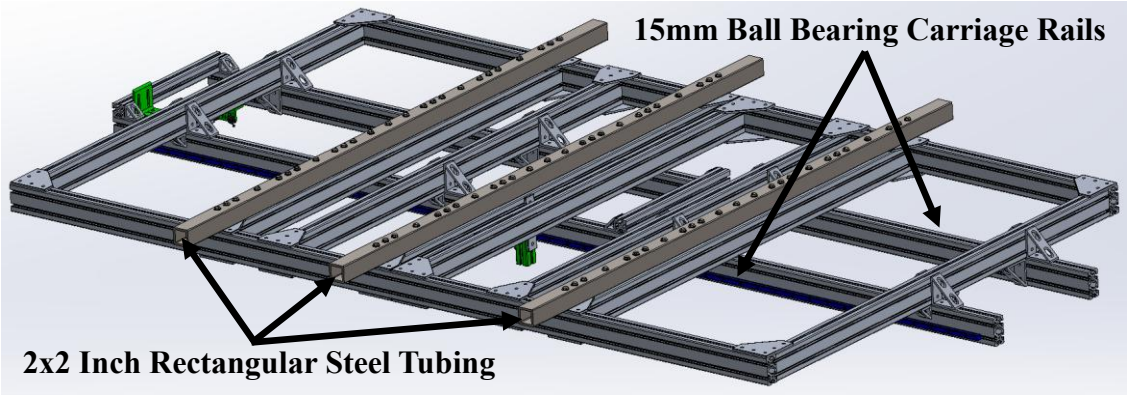

Figure 3. Main apparatus frame

The outer dimensions of the ice box measured 1580 mm in length, 522 mm in width, and 565 mm in height. Figure 4 and Figure 5 illustrate the ice box which contained a pressure plate that moved back and forth along a set of linear bearings. As shown in Figure 5, the rear section of the ice box housed two pneumatic pistons that actuated the pressure plate, enabling it to press the ice against the friction board. The ice box was designed to traverse the length of the tank along 15 mm carriage rails, driven by a lead screw connected to a small electric motor, as depicted in Figure 6. The associated lead screw nut, which was secured to the ice box using a mounting bracket, can be seen in Figure 4 and Figure 5. Four mounting brackets attached the ice box to the main apparatus frame using eight 15 mm linear motion ball-bearing carriages. The motor assembly utilized a lead screw mechanism to move the ice box along the tank. Additionally, limit switches were installed on the frame at both ends of the tank to interface with the lead screw nut mount. These switches facilitated system homing and ensured the safe operation of the apparatus.

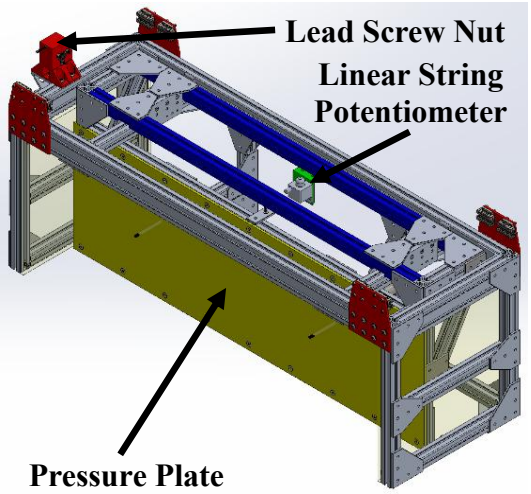

Figure 4. Ice box front view

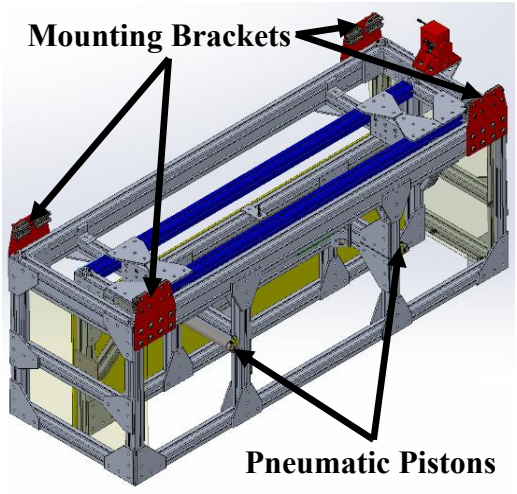

Figure 5. Ice box back view

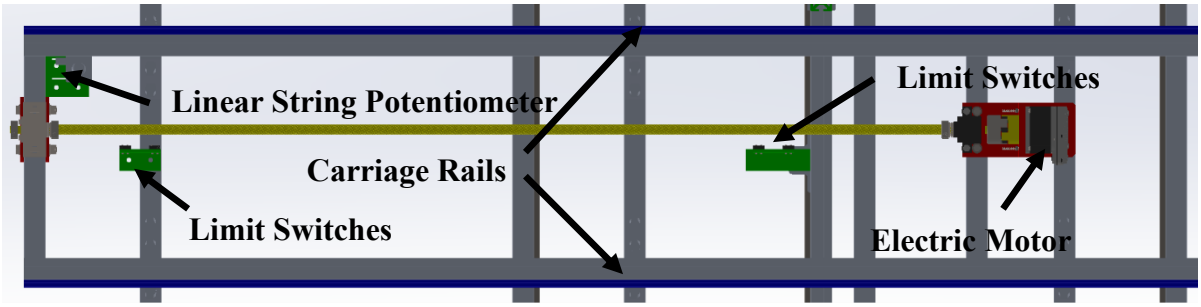

Figure 6. Motor assembly and carriage rails bottom view

The friction board was fixed to a frame that was suspended from the main apparatus structure. This frame was mounted to five flex links and six load cells. Each flex link was designed for the purpose of preventing load transfer in two of the three (3) cartesian coordinates while simultaneously constraining movement and allowing force measurement in the third. This isolates each of the load cells from influencing the measurements of other load cells in the system. There are six degrees of freedom, these being the three (3) cartesian coordinates represented by axis x, y and z, with their corresponding rotational degree of freedom for each. Therefore, to properly constrain and measure force in all degrees, six (6) load cells were used, one for each degree of freedom. Although other load cell implementations may have been credible, with the given size constraints, the design chosen was seemingly the simplest way to effectively constrain all degrees of freedom while allowing force measurements for each.

Two (2) of the 500 kg (1102 lbs) round button type load cells, Fz_1 and Fz_3, were mounted vertically on either side of the friction board assembly near the friction board. Another vertically oriented button-type load cell, Fz_2, was positioned at the centre of the friction board assembly, as shown in Figure 7. These vertical load cells measure forces in the z-axis and support the weight of both the friction board and the air bubbler assemblies, while also preventing the friction board assembly from rotating around the horizontal axes (x-axis and y-axis). The remaining two button type load cells, Fy_4 and Fy_5, were mounted horizontally, perpendicular to the plane of the friction board, and positioned at either end of the friction board assembly. These load cells measured the force applied in and out of the friction board in the y-axis, while also restricting rotation around the vertical axis (z-axis). Given the relatively low magnitude of longitudinal ice drag forces expected along the x-axis, the use of a 500 kg button-type load cell and corresponding flex links was deemed inappropriate. Instead, a 25 kg (50 lb) shear beam-type load cell Fx_{6A}, paired with a ball joint swivel, was used to measure force in this direction. This load cell was mounted as close to the friction board surface as possible to mitigate eccentricity loading caused by the transverse drag force of the ice, positioned just above the friction board, between the friction board frame and the moving ice box. The positions and orientations of all load cells are detailed in Figure 7.

The surface of the friction board was coated with a specialized paint to achieve a standard hull-ice friction coefficient of 0.05. This coefficient was selected to ensure direct correlation with past model testing results (Spencer & Jones, 2001; Lau, 2015). The friction board had a length of 2950 mm and a height of 400 mm, to optimize the usable surface area to enable the attainment of steady-state conditions.

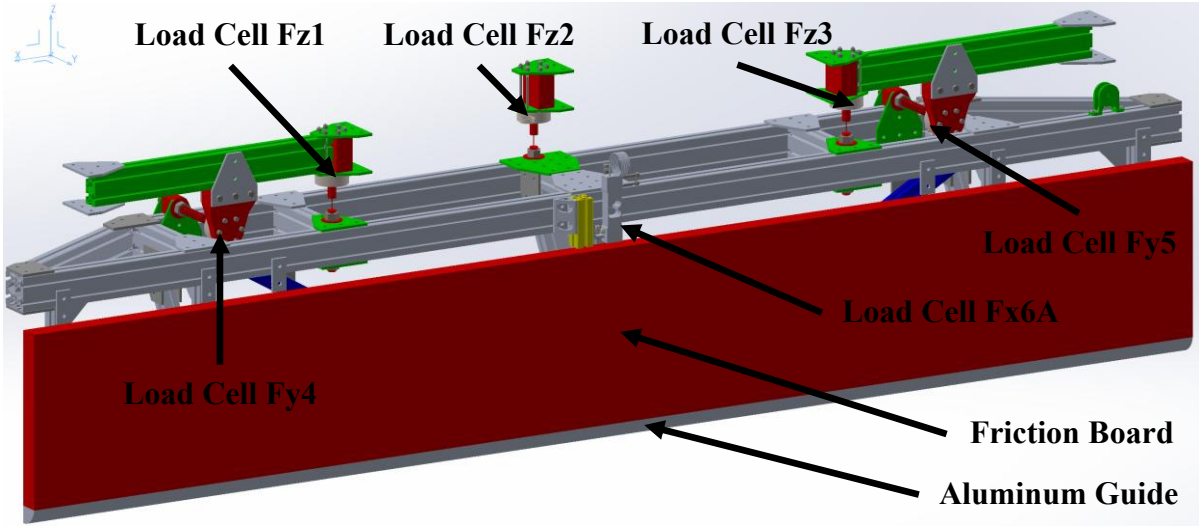

Figure 7. Friction board assembly

Scale-model testing of aeration bubbler plumes has provided valuable insight into the potential approaches for scaling air bubbler systems (Bombardelli, et al., 2007). However, the specific application of scaling an air bubbler system to reduce ice resistance in this configuration had not been previously investigated. As a result, for a starting point in this area of study, it was decided the preliminary system setup employed geometric scaling based on the physical dimensions of the CCGS Henry Larsen (i.e. port size, spacing, and depth). Future iterations of this type of setup investigating the direct correlation of ice drag force between an air bubbler at model scale and full scale could be a valuable topic to investigate but is beyond the scope of this paper.

The air bubbler system was mounted along the bottom of the friction board assembly and consisted of 31 ports distributed along its full length, as illustrated in Figure 8. In the full-scale vessel, 16 ports were installed on each side of the hull, with operational flexibility allowing deployment from as few as 8 ports (Wang, et al., 2023) For this apparatus, the number and spacing of ports were increased to ensure complete coverage of the test section. The system utilized a 1-¼" NPT pipe that extended the length of the friction board assembly. Air was supplied to both ends of the pipe via an external flow control system connected through airline fittings. Each port in the system comprised three right-angle fittings arranged in a C-bend configuration and threaded into the underside of the pipe at regular intervals. This configuration, resembling a sink trap, allowed air to be discharged while preventing water ingress into the system. The pipe functioned as a low-pressure reservoir. As air accumulated, internal pressure built up until it exceeded the hydrostatic head at the port depth, at which point air was released through the ports. It was critical that all ports were positioned at an equal depth to maintain uniform head pressure, thereby ensuring consistent flow distribution across the system. To prevent bubbles from migrating behind the friction board, an aluminum guide was installed at the bottom of the assembly. This guide also served to reinforce the structure of the friction board, as shown in Figure 7.

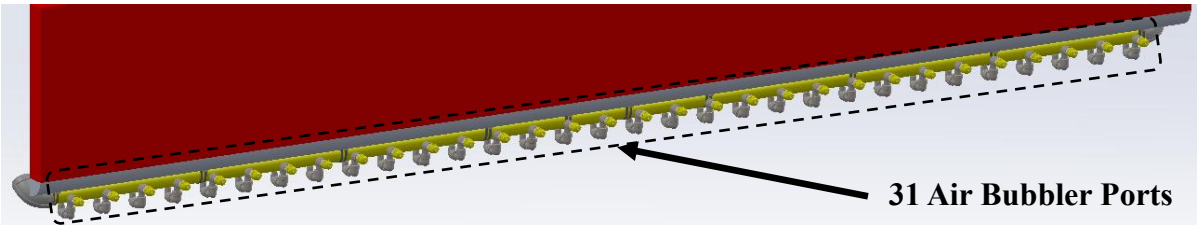

Figure 8. Air bubbler system

INSTRUMENTATION

The test equipment utilized an array of digital and analog sensors to capture key experimental data. The digital data included measurements of current, position, and motor speed, which were recorded by the motor controller and transmitted to a Data Acquisition System (DAS). Additionally, a digital signal was sent over the network from the NRC servers to the DAS, ensuring universal time synchronization across all recorded data. The analog instrumentation comprised six load cells, an airflow rate potentiometer, a pressure sensor, two string potentiometers, and a wave probe sensor to determine water level. The measurement ranges and operating temperatures for these sensors are detailed in Table 1.

Table 1. List and specifications of sensors

Sensor name	Sensor range		Temperature range		Accuracy
	Maximum	Minimum	Maximum	Minimum	
Round threaded through hole load cell	500kg (1102lbs)	-500kg (1102lbs)	60°C (140°F)	−18°C (0°F)	±250g (±8.8oz)
Rectangle beam load cell	20kg 44lb	-20kg (-44lb)	38°C (100°F)	−9°C (15°F)	±4g (±0.14oz)
Linear motion position transmitter	127cm (50")	0m (0")	71°C (160°F)	−18°C (0°F)	±0.25%
Indicating flow meter with analog outputs	708L/min (25SCFM)	56.6L/min (2SCFM)	116°C (240°F)	−29°C (−20°F)	±2%
NP400 pressure transmitter	10bar (145psig)	0bar (0psig)	70°C (158°F)	−20°C (−4°F)	±0.5%

Load Cells and Force Measurement

The test apparatus incorporated six load cells to measure forces in all axes. Five (5) of these sensors were 500 kg (1102 lbs) round, threaded through-hole button-type load cells, while the sixth was a 25 kg (50 lbs) shear beam-type load cell. Both sensor types were capable of measuring forces in tension and compression, enabling the button-type load cells to be interchangeable within the flex link mounts. As previously discussed, the flex links allow for the load cell to measure load in there given direction without influencing the values recorded in other load cells. Additionally, the flex links were designed to act as mechanical fail safes, failing under overload conditions before damage could occur to the load cells themselves, therein protecting the more costly sensors. A smaller shear beam-type load cell, designated

Fx_{6A}, was utilized due to spatial and positional constraints within the test apparatus. This sensor was specifically implemented to measure the ice friction forces acting on the friction board. Given that these forces were significantly lower in magnitude compared to those measured by the other load cells, a 25 kg (50 lbs) model was deemed appropriate for this application. The placement and orientation of all load cells are illustrated in Figure 7.

Position Measurement

To accurately determine the position of both the pressure plate and the ice box within the tank, two linear string potentiometers were implemented. One potentiometer was mounted at the end of the tank and secured to the main apparatus frame. This sensor measured the full range of ice box motion, from 0 mm to just over 1000 mm. The recorded data was cross-referenced with digital motor position data to ensure accuracy. The second linear string potentiometer was mounted inside the ice box, positioned behind the pressure plate. The string end was attached to the top of the pressure plate, allowing it to measure the plate's displacement within a range of approximately 0 mm to 140 mm. These components are illustrated in Figure 4 and Figure 6.

Air Bubbler System Monitoring

To monitor the air flow rate throughout testing, an Omega FLR6725D flow meter was implemented. The flow meter, along with the air control system, was mounted outside the tank. It had the capability to record airflow as low as two (2) SCFM (56.6 L/min) and up to a maximum of 25 SCFM (708 L/min). Airflow adjustments were made using a flow-adjustment valve, which allowed for precise control between tests to account for varying conditions.

Ice Pressure Simulation

Pack ice pressure was simulated using two small pneumatic pistons, which provided a steady and consistent force on the ice throughout testing. The piston pressure was monitored continuously, and the resulting ice pressure was calculated based on the recorded values. A 10-bar (145 PSIG) NP400 pressure transmitter was used to capture piston pressure data. This pressure sensor was mounted on the side of the tank alongside the pressure control valve. The transmitter was threaded into the pressure-regulating valve via a ¼ inch NPT port, with an additional manual pressure gauge installed downstream of the regulator using a T-fitting for verification.

Water Depth Monitoring

A wave probe was utilized to measure the water depth within the tank. This probe, developed by the NRC and based on the commercially available Akamina Technologies AWP-24-3 system, was originally implemented by the NRC for recording wave heights in their wave tank. The probe operates by measuring the capacitance along a known length of wire, which varies as the water level rises or falls along its length. These capacitance changes are processed through a digital algorithm, converting the output into a linear analog voltage signal that can be interpreted by the DAS. The resulting data provides a precise measurement of water level variations within the tank.

CALIBRATION

Three different calibration methods were implemented for the sensors in this design: in-situation calibration, calibration on a test bench, and data sheet calibration using manufacturer specifications. The choice of method depended on the specific sensor and its role in the system.

Beam Type Load Cell Calibration

For the beam load cell Fx_{6A}, an in-situation calibration was deemed necessary, as it measures the translational force of ice against the friction board. The structural characteristics of the test frame could influence its output, making a direct, system-integrated calibration more reliable. This approach ensured that any effects from the test frame were accounted for. To prevent hysteresis near zero, the load cell was preloaded in the direction of the expected ice drag force and then re-zeroed in the DAS. Calibration weights were attached to a bolt mounted at the top centre of the friction board frame, using a cable and pulley system to simulate the ice frictional force. An inline S-type load cell was installed between the cable and bolt to measure the applied force. The cable was routed through three pulleys, which guided it from the top of the friction board frame to the side of the tank, before directing it downward outside the tank, where calibrated weights could be suspended. The measured force from the S-type load cell was cross-referenced with the known calibrated weights. Due to potential dynamometer system inaccuracies, the beam-type load cell Fx_{6A} was calibrated based on the output of the S-type load cell. While this method introduced a potential compounding of inaccuracies from both load cells, it was deemed an acceptable trade-off to maintain overall system accuracy under operational conditions. The calibration range for Fx_{6A} was set between 48.33 N and 125.40 N. The percent error was calculated as 0.104% of the range, corresponding to an absolute error of 0.0799 N. Figure 9 illustrates the calibration range used for load cell Fx_{6A}.

Table 2. Load cell Fx_{6A} calibration x-pull

Data Point	Calibration weight (kg)	Physical value (N)	Measured value (Volts)	Fitted Curve value (N)	Error (N)
1	6.00	48.33	-0.0022	48.26	-0.07
2	8.50	66.99	-0.0028	66.07	0.08
3	11.00	87.60	-0.0035	87.64	0.04
4	13.50	106.17	-0.0041	106.13	-0.04
5	16.00	125.40	-0.0048	125.47	-0.01

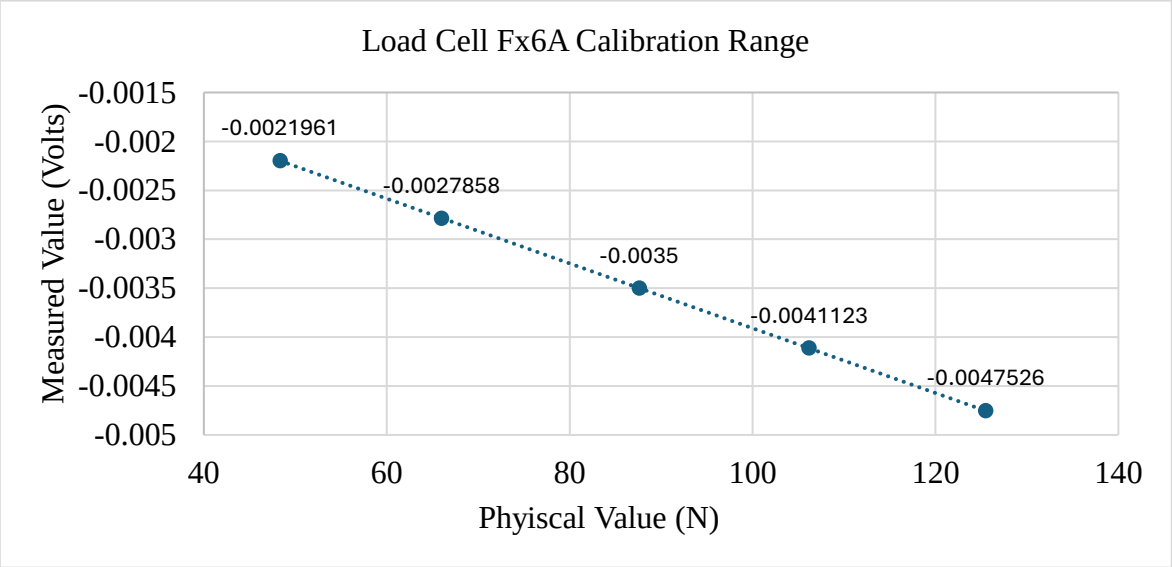

Figure 9. Load cell Fx_{6A} calibration range

Wave Probe Calibration

An in-situation calibration method was used for the wave probe to ensure accurate water level measurements. Before installation, calibration marks were made at five-centimeter increments along the external metal rod using a calibrated measuring tape. The tank's water level was set, and the wave potentiometer was systematically lowered and re-mounted at each marked position. At each point, the corresponding voltage output was recorded and assigned in the DAS. After all the calibration points were recorded, the wave potentiometer was mounted in its final position at the middle of its operational range to minimize measurement errors, and the calibration values closely followed a linear trend. The tank was then filled to the precise level required for testing. To establish a reliable reference point, this water level was measured with a calibrated measuring tape from the bottom of the tank to the waterline, confirming a depth of 620 mm. The wave potentiometer was then zeroed to this value, ensuring accurate depth readings throughout the testing process.

Button Type Load Cell Calibration

The five 500 kg (1102 lbs) round threaded through-hole button-type load cells could not be calibrated in-situation due to the substantial force required and the logistical challenges of applying these forces without affecting or potentially damaging the test frame. Since all these load cells were newly acquired, the manufacturer's calibration data was used instead. These load cells were designed to measure both tension and compression, with voltage-to-force data provided for each measurement mode. To perform the calibration, the DAS was connected to a power supply that was programmed to deliver a constant voltage. The voltage was systematically adjusted to match the load points specified in the manufacturer's data sheet, and the corresponding load force values were entered into the DAS as calibration points. This process ensured that the calibration data was correctly registered within the DAS while being processed through the provided Programmable Logic Controller (PLC). To prevent interference and improve accuracy, a separate power supply was used for each load cell, effectively isolating them from one another. For testing purposes, all load cells, including the 20 kg (44 lbs) rectangular beam load cell, were connected to the DAS through an isolation box. This additional step helped minimize electrical noise in the data, ensuring more reliable and precise force measurements.

String Potentiometer Calibration

The linear motion position transmitter was calibrated using a test bench setup. It was first mounted onto a purpose-built calibration frame designed for different types of linear motion transmitters. This frame consisted of a mounting plate and an extendable, lockable rod, which was precisely marked in increments using a calibrated tape measure. By locking the rod at specific positions, the transmitter was able to record steady-state data for calibration. The rod was then extended incrementally, allowing for various calibration points to be entered into the DAS. As previously noted, the DAS data recorded for the ice box position using the linear motion position transmitter was cross-referenced with the digital position and velocity data from the motor controller. Even at full extension, the discrepancy between the two measurements was found to be less than one millimeter, confirming the accuracy of the calibration. After completion, the position transmitter was re-zeroed in the test frame following the homing of the motor on the right side of the tank.

Air Flow Meter Calibration

The indicating air flow meter was calibrated on a test bench before being installed in the testing apparatus. It was connected to the ball and flow rate valve setup intended for use during testing.

The meter was configured to operate in the appropriate mode for air at standard temperature. Calibration was conducted using air supplied by the NRC's building air system through standard air hoses. The meter's analog outputs were used to transmit voltage data to the DAS, where the information was processed. Since the flow meter had an onboard calibration provided by the manufacturer, the display values from the meter were recorded as calibration points in the DAS after the system reached a steady state. The accuracy of the flow rate calculations depended on maintaining a stable air temperature within the system, as the pre-set temperature value was programmed into the flow meter. To ensure consistency, the air compressor used for testing was placed outside the test room in a controlled-temperature environment. After completing the calibration process in the DAS, the air flow meter was mounted onto the apparatus and prepared for testing.

Pressure Transmitter Calibration

Lastly, the pressure transmitter was also calibrated. This sensor was responsible for measuring air pressure within the pneumatic system, which was then used to calculate the applied force on the ice. Rather than requiring an absolute pressure measurement within the system, the calibration focused on establishing a consistent relationship between the pressure recorded by the sensor and the force applied. To achieve this, the pressure transmitter's maximum output voltage was set to correspond with its maximum pressure specification of 10 bar (145 psi). A manual pressure gauge was used to verify the transmitter's repeatability and ensure it remained within the correct range. To determine the appropriate pressure levels for testing, the system was initially set up in the ice box before being positioned inside the tank. The same S-type load cell used for the X-pull calibration of the 20 kg (44 lbs) rectangular beam load cell was installed between the back of the ice box and the pressure plate, secured with two I-bolts at either end. The pressure in the system was adjusted, and after a 10-minute settling period, the force recorded by the S-type load cell was measured. This force measurement was then used to establish the expected force corresponding to each set pressure level. The 10-minute waiting period allowed the pneumatic system and pressure plate to stabilize, ensuring that the force readings remained consistent. This same procedure was followed before every test run to maintain uniform force application on the ice by the pressure plate.

SAMPLE RESULTS FROM INTIAL TEST

While a detailed discussion of test results is beyond the scope of this paper, and are reported in a companion paper, a brief discussion of sample data is provided here to offer insight into the performance of the dynamometer. This section examines processed example data from one of the test runs. All data presented was taken while the ice box was positioned between 200 mm and 800 mm. This range was selected to allow the ice box sufficient time to accelerate and decelerate at the beginning and end of the test, ensuring that the system reached a steady-state condition. Additionally, this delay was necessary to allow the water, disturbed by the motion of the ice box, to stabilize into a steady hydrodynamic state. Focusing on data within this range also ensured that any position-related characteristics of the test frame influencing the results remained comparable across all test runs. Test run 94 serves as an example of a low-speed test (58 mm/s) conducted at a medium ice pressure (374 Pa), with the air bubbler flow turned off. This test is representative of other runs performed under similar conditions. Figure 10 illustrates the measured force recorded by the Fx_{6A} load cell during test run 94, specifically within the ice box position range of 200 mm to 800 mm. The recorded data shows a linear increase in load over the course of the test, despite the ice box maintaining a constant velocity of 58 mm/s within this time window. This result is unexpected; it could have been predicted

that the recorded force would have a constant load across the deration of the test run. This steady increase in loading may have been a result of the friction board placement in the tank in relation to the movement of the ice box. Even the slightest misalignment could have drastic effects on the recorded forces. However, as this trend is consistent and repeatable across testing, values between the bubbler on and off can be compared. For future testing, improved manufacturing precision and alignment of the friction board and ice box, and/or replacing the ball joint swivel on load cell Fx_6A with a wire connection, could help reduce such effects and enhance measurement accuracy. In Figure 10 the data also exhibits oscillations throughout the test run, seen for example between 26.4 s to 28 s and again from 28 s to 29.8 s. Given that the motor and its controller power supply were isolated through a battery bank, it is unlikely that electrical noise was responsible for these oscillations. Instead, the observed variations in force are more likely the result of a physical phenomenon inherent to the test setup.

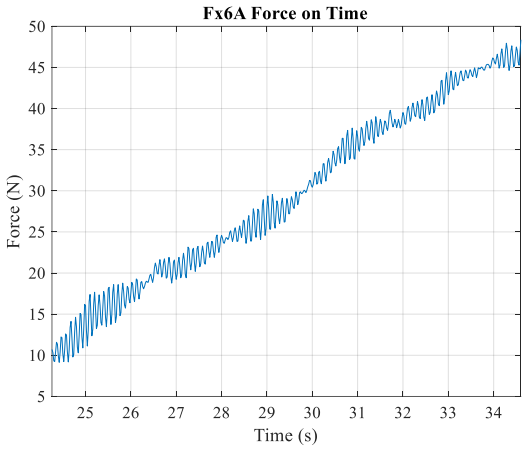

Figure 10. Run 94 force on load cell Fx_{6A} between ice box position 200mm to 800mm

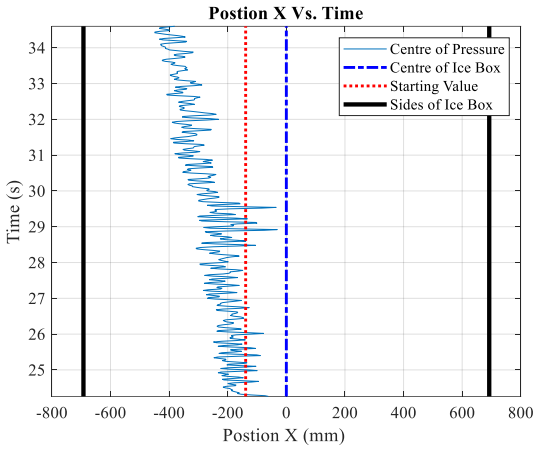

Figure 11. Run 94 centre of pressure in the X-axis

Figure 11 illustrates the centre of pressure along the x-axis during test run 94, calculated using a system of equations based on the forces measured from all load cells. The vertical dashed line represents the centre of the ice box, while the solid vertical lines indicate its sides. The vertical dotted line marks the initial centre of pressure at the start of the test. As shown in the figure, the centre of pressure shifts toward the left side of the ice box as the test progresses. This suggests that the distribution of brash ice in the box or the load transmission paths through the ice may be affected as the ice box moves through the tank. The observed change in ice distribution may be influenced by agitation of the ice by the bubbler which causes it to shift from its initial position. This shift in the centre of pressure may contribute to the force recorded by the Fx_{6A} load cell.

CONCLUSION

Designing a dynamometer to measure the effects of an air bubbler system on ice resistance on a ship hull, which is sensitive enough to accurately record and quantify changes in ice drag force on a friction board is a complex and challenging task. Many valuable lessons were learned from this project, which ultimately led to the development of a dynamometer that can evaluate the effects of an air bubbler system on model scale ice-hull surface friction forces. The insights gathered from this design process and subsequently during testing (please see companion paper for more detail, (Osmond, et al., 2025)), provide exciting new opportunities to gain deeper

understanding of the complex air-ice-water-hull interaction processes and the functionality of the air bubbler system itself. This design represents a significant step forward in friction board testing and introduces a new method for evaluating ice friction and studying the effects of ice pressure on ship performance in brash ice. Future iterations of this type of dynamometer offers a promising avenue for supporting further development of technology for enhancing the performance of ice class ships and air bubbler systems. Through such research, improvements to ship performance, fuel efficiency, and the design tools available can be achieved. This ultimately leads to more effective ice management strategies and safer navigation in ice-covered waters. This work lays the foundation for further refining ice resistance mitigation techniques and contributes to providing a reliable methodology for assessing and optimizing ice friction reduction systems.

REFERENCES

Bombardelli, F. A. et al., 2007. Modeling and scaling of aeration bubble plumes: A two-phase flow analysis. *Journal of Hydraulic Research,* 45(5), pp. 617-630.

Browne, T. & Wang, J., 2023. *Hull-ice friction: Correlating model hull friction to resistance in ice.* Ottawa, Ontario, Canada, International Society of Offshore and Polar Engineers (ISOPE).

Hill, B., 2008. *Environmental Modeling - Ice 42-8595-S/GM-4,* s.l.: INSTITUTE FOR OCEAN TECHNOLOGY.

Juurmaa, K., 1978. The Wartsila Air Bubbling System. *Polar Record,* 19(119), pp. 121-127.

Lau, M., 2015. *Model-scale/full-scale correlation of NRC-OCRE's model resistance, propulsion and maneuvering test results.* St. John's, Newfoundland and Labrador, Canada, NRC Publications Archive.

Marmo, B. A., Blackford, J. R. & Jeffree, C. E., 2005. Ice friction, wear features and their dependence on sliding velocity and temperature. *Journal of Glaciology,* 51(174), pp. 391-398.

Osmond, N. M., Wang, J. & Taylor, R. S., 2025. *Assessment of the Effectiveness of Air Bubbler Systems in Reducing Hull-Ice Interaction Loads.* St. John's, Newfoundland and Labrador, Canada, Port and Ocean of Engineering under Arctic Conditions (POAC 2025).

Spencer, D. & Jones, S. J., 2001. Model-scale/full-scale correlation in open water and ice for Canadian Coast Guard "R-Class" icebreakers. *Journal of Ship Research,* 45(4), pp. 249 - 261.

Wang, J. et al., 2023. *Performance Evaluation of CCGS Icebreaker Henry Larsen with Air Bubbler System in Ice,* St. John's, Newfoundland and Labrador, Canada: National Research Council Canada.

Wilkman, G., 2011. *Experience of Air Bubbling System in Ice Navigation and Future Possibilities.* Houston, Texes, USA, Offshore Technology Conference.